ARTICLE

Loss of VPS13C Function in Autosomal-Recessive Parkinsonism Causes Mitochondrial Dysfunction and Increases PINK1/Parkin-Dependent Mitophagy

Suzanne Lesage,[1,2,3,4,25] Valérie Drouet,[1,2,3,4,25] Elisa Majounie,[5,25] Vincent Deramecourt,[6] Maxime Jacoupy,[1,2,3,4] Aude Nicolas,[1,2,3,4] Florence Cormier-Dequaire,[1,2,3,4,7] Sidi Mohamed Hassoun,[1,2,3,4] Claire Pujol,[1,2,3,4] Sorana Ciura,[1,2,3,4] Zoi Erpapazoglou,[1,2,3,4] Tatiana Usenko,[1,2,3,4] Claude-Alain Maurage,[6] Mourad Sahbatou,[8] Stefan Liebau,[9] Jinhui Ding,[5] Basar Bilgic,[10] Murat Emre,[10] Nihan Erginel-Unaltuna,[11] Gamze Guven,[11] François Tison,[12] Christine Tranchant,[13] Marie Vidailhet,[1,2,3,4,14] Jean-Christophe Corvol,[1,2,3,4,7] Paul Krack,[15] Anne-Louise Leutenegger,[16,17] Michael A. Nalls,[5] Dena G. Hernandez,[5] Peter Heutink,[18] J. Raphael Gibbs,[5] John Hardy,[19] Nicholas W. Wood,[19] Thomas Gasser,[18] Alexandra Durr,[1,2,3,4,20] Jean-François Deleuze,[21] Meriem Tazir,[22] Alain Destée,[23] Ebba Lohmann,[10,24] Edor Kabashi,[1,2,3,4] Andrew Singleton,[5] Olga Corti,[1,2,3,4,*] Alexis Brice,[1,2,3,4,20,*] French Parkinson's Disease Genetics Study (PDG), and the International Parkinson's Disease Genomics Consortium (IPDGC)

Autosomal-recessive early-onset parkinsonism is clinically and genetically heterogeneous. The genetic causes of approximately 50% of autosomal-recessive early-onset forms of Parkinson disease (PD) remain to be elucidated. Homozygozity mapping and exome sequencing in 62 isolated individuals with early-onset parkinsonism and confirmed consanguinity followed by data mining in the exomes of 1,348 PD-affected individuals identified, in three isolated subjects, homozygous or compound heterozygous truncating mutations in *vacuolar protein sorting 13C* (*VPS13C*). *VPS13C* mutations are associated with a distinct form of early-onset parkinsonism characterized by rapid and severe disease progression and early cognitive decline; the pathological features were striking and reminiscent of diffuse Lewy body disease. In cell models, VPS13C partly localized to the outer membrane of mitochondria. Silencing of *VPS13C* was associated with lower mitochondrial membrane potential, mitochondrial fragmentation, increased respiration rates, exacerbated PINK1/Parkin-dependent mitophagy, and transcriptional upregulation of *PARK2* in response to mitochondrial damage. This work suggests that loss of function of VPS13C is a cause of autosomal-recessive early-onset parkinsonism with a distinctive phenotype of rapid and severe progression.

Introduction

Parkinson disease (PD [MIM: 168600]) is a motor syndrome with variable combinations of akinesia, rigidity, and rest tremor responding to levodopa. It is caused by degeneration of the dopaminergic neurons in the substantia nigra pars compacta and is associated with Lewy bodies, intraneuronal inclusions enriched in α-synuclein. In recent years, our understanding of the pathophysiological mechanisms underlying molecular defects in familial forms of PD has greatly advanced. Three genes have been conclusively associated with autosomal-dominant (AD) forms of PD (*SNCA* [MIM: 163890], *LRRK2* [MIM: 609007], and *VPS35* [MIM: 601501]) and eight genes (*PARK2* [MIM: 602544], *PINK1* [MIM: 608309], *DJ-1* [MIM: 602533], *ATP13A2* [MIM: 610513], *FBXO7* [MIM: 605648], *PLA2G6* [MIM: 603604], *SYNJ1* [MIM: 604297], and *DNAJC6* [MIM: 608375]) with early-onset (EO) autosomal-recessive (AR) forms.[1] EO AR parkinsonism is clinically and genetically heterogeneous: mutations in *PARK2*, *PINK1*, and *DJ-1* cause phenotypes similar to idiopathic PD with good and prolonged response to dopaminergic

[1]Sorbonne Universités, UPMC Université Paris 6 UMR S 1127, 75013 Paris, France; [2]Inserm U 1127, 75013 Paris, France; [3]CNRS UMR 7225, 75013 Paris, France; [4]Institut du Cerveau et de la Moelle épinière, ICM, 75013 Paris, France; [5]Laboratory of Neurogenetics, National Institute on Aging, NIH, Bethesda, MD 20892, USA; [6]Department of Histology and Pathology, University of Lille Nord de France, Lille University Hospital, 59000 Lille, France; [7]Centre d'Investigation Clinique Pitié Neurosciences CIC-1422, 75013 Paris, France; [8]Fondation Jean Dausset-CEPH, 75010 Paris, France; [9]Institute of Neuroanatomy, Eberhard Karls University Tübingen, 72074 Tübingen, Germany; [10]Behavioural Neurology and Movement Disorders Unit, Department of Neurology, Istanbul Faculty of Medicine, Istanbul University, 34390 Istanbul, Turkey; [11]Department of Genetics, Institute for Experimental Medicine, Istanbul University, 34390 Istanbul, Turkey; [12]Institut des Maladies Neurodégénératives, Université de Bordeaux et CHU de Bordeaux, 33000 Bordeaux, France; [13]Pôle Tête-Cou-CETD, Service de Neurologie, Hôpitaux Universitaires, 67000 Strasbourg, France; [14]Pôle des Maladies du Système Nerveux, Fédération de Neurologie, Hôpital de la Salpêtrière, 75013 Paris, France; [15]Neurology Department, CHU de Grenoble, Joseph Fourier University, and INSERM U836, 38000 Grenoble, France; [16]Inserm U946, 75010 Paris, France; [17]Université Paris Diderot, Institut Universitaire d'Hématologie, UMR946, 75010 Paris, France; [18]Hertie Institute for Clinical Brain Research, University of Tübingen and DZNE, German Center for Neurodegenerative Diseases, 72074 Tübingen, Germany; [19]Department of Molecular Neuroscience, UCL Institute of Neurology, London WC1N 3BG, UK; [20]Department of Genetics and Cytogenetics, AP-HP, Hôpital de la Salpêtrière, 75013 Paris, France; [21]Commissariat à l'Energie Atomique, Institut Génomique, Centre National de Génotypage, 91000 Evry, France; [22]Service de Neurologie CHU Mustapha, 16000 Alger, Algérie; [23]Movement Disorders Unit, Lille University, Inserm U837, Lille University Hospital, 59000 Lille, France; [24]Department of Neurodegenerative Diseases, Hertie Institute for Clinical Brain Research, University of Tübingen, and DZNE, German Center for Neurodegenerative Diseases, 72076 Tübingen, Germany
[25]These authors contributed equally to this work
*Correspondence: olga.corti@upmc.fr (O.C.), alexis.brice@upmc.fr (A.B.)
http://dx.doi.org/10.1016/j.ajhg.2016.01.014.

therapy. Other EO AR PD-associated genes cause more severe disease, a poor response to levodopa, and additional clinical signs, such as dystonia and cognitive impairment.[1] Mutations in *PARK2* and *PINK1* are the most common cause of EO AR PD, accounting for ~50% and 4% of familial cases in Europe, respectively.[2,3] A significant proportion of cases remain genetically unexplained.

EO AR PD is linked to mitochondrial dysfunction. The mitochondrial kinase PINK1 and the E3 ubiquitin-protein ligase Parkin cooperate in mitochondrial quality control.[4] They promote the removal of dysfunctional mitochondria in a process termed mitophagy that might also involve FBXO7.[4,5] In addition, they play a role in a vesicular trafficking pathway targeting damaged mitochondrial components to the lysosome.[6] To identify additional PD-associated genes involved in AR EO parkinsonism, we performed homozygosity mapping and exome sequencing in consanguineous PD families and isolated individuals and used data mining in the exomes of 1,348 unrelated PD-affected individuals. Five truncating mutations in *vacuolar protein sorting 13C* (*VPS13C* [MIM: 608879]) were identified in three unrelated PD-affected isolated individuals. We provide evidence that depletion of VPS13C exacerbates mitochondrial vulnerability to stress.

Subjects and Methods

Participants

Gene Discovery Cohort

We selected nine PD-affected families (with two or more affected siblings) and 43 unrelated isolated individuals according to the following criteria: (1) diagnosed by neurologists according to the UK Parkinson's Disease Society Brain Bank (PDSBB) clinical diagnostic criteria[7] and onset $\leq$55 years in at least one affected family member; (2) with no mutations in known PD-associated genes; and (3) with confirmed consanguinity (inbreeding coefficient $F \neq 0$ computed with the FEstim program[8]). Sixteen families or isolated subjects were European, 16 North African, 19 Turkish, and 1 Lebanese. A total of 66 PD-affected individuals (23 family members and 43 isolated subjects) and 39 unaffected relatives were included for the genome-wide screen study. 62 affected and 10 unaffected individuals were subsequently selected for whole-exome sequencing.

Validation Cohort

Exome data were obtained from a series of 1,348 additional PD-affected individuals (99% unrelated, 99% of European ancestry, 60% males, mean age at onset 41.7 ± 11.0 years), including 249 French PD-affected probands (57% males, age at onset $\leq$ 40 years, 50 individuals with atypical forms of parkinsonism) recruited by the French network for the study of PD genetics (PDG) and 530 matched control subjects (95% of European ancestry, 65% males, mean age at examination: 45.1 ± 10.7 years) from the International Parkinson Disease Genomics Consortium (IPDGC).

100 Turkish control subjects without family history of PD (43% males; mean age at examination, 60.4 ± 13.9 years) served to check for the absence of the identified variant in family A, which originated from Turkey.

A flow diagram detailing the selection criteria of PD-affected individuals and control subjects and the different experimental steps of the study is provided (Figure S1).

Study Approval

Informed consent was obtained from all participants, and the genetic studies were approved by local ethics committees (INSERM, CCPPRB du Groupe Hospitalier Pitié-Salpêtrière, Paris, France).

Neuropathological Assessment

The autopsy of the affected individual II-1 in family B (Figure 1) was performed approximately 36 hr post mortem. Brain tissues were fixed for 6 weeks in 10% buffered formalin, extensively sampled, and processed as previously described.[9] Immunohistochemistry was performed by a Ventana Benchmark automate. We used hematoxylin-eosin staining for histopathology. For immunochemistry, the antibodies used were: anti-Tau (in-house AD2,[10] 1 ng/mL), anti-β-amyloid (4G8, 1:1,000, Sigma), anti-α-synuclein (LB509, 1:500, Abcam), anti-ubiquitin (1:1,000, Dako), anti-TDP-43 (1:500, Protein Tech), and anti-glial fibrillary acid protein (GFAP, 1:20,000, Dako). The degree of neuronal loss and the frequency of α-synuclein-immunoreactive and other inclusions were determined semiquantitatively by visual inspection, in comparison to brains of three age-matched controls (two males and one female) from the Lille Neurobank collection.

Molecular Studies

Whole-Genome Homozygosity Linkage Mapping

Genome-wide screens were performed on all available affected (n = 66) and unaffected (n = 39) individuals from the gene discovery cohort using the Illumina HumanCytoSNP-12 v2.1 DNA Analysis BeadChip microarrays that contain ~300,000 SNPs and ~1,300 markers of common copy-number variations (CNVs). Homozygosity tracks (>2 Mb) were visualized with the Homozygosity Detector module and CNV with the Illumina cnvPartition module. The inbreeding coefficients F were computed with the FEstim program.[8] Samples from individuals with confirmed consanguinity ($F \neq 0$) were subjected to exome sequencing.

Whole-Exome Sequencing

Exons from 62 affected (19 relatives and 43 isolated individuals) and 10 unaffected family members from the gene discovery cohort and all the 1,348 affected and 530 control individuals from the validation cohort were captured using different exome enrichment kits from fragmented genomic DNA and sequenced as indicated in Table S1. 10-fold mean sequencing depth was achieved in 96.4% and 88.8% of baited regions in PD-affected individuals and control subjects, respectively, and 30-fold mean sequencing depth was achieved across ~75% of targeted regions.

Human reference sequence UCSC hg19 was used for sequence alignment and variant calling with the Burrows-Wheeler Aligner[11] and the Genome Analysis Toolkit.[12] PCR duplicates were removed prior to variant calling using Picard software. Variants were annotated with ANNOVAR software[13] (exomes from validation cohort) or SnpEff and SnpSift programs (exomes from gene discovery cohort). Data were analyzed with Ingenuity Variant Analysis (IVA) TM software from Ingenuity System. Effects on mRNA splicing by putative splice variants (±5 base pairs around splice junctions according to IVA threshold) were analyzed with Splice Site Finder, MaxEntScan, NNsplice, Genesplicer, and Human Splicing Finder,[14–16] all included in Alamut v.3 software. The human VPS13C protein and its closest homologs were aligned with Alamut v.3 software, computed by Ensembl, and aligned with MUSCLE.

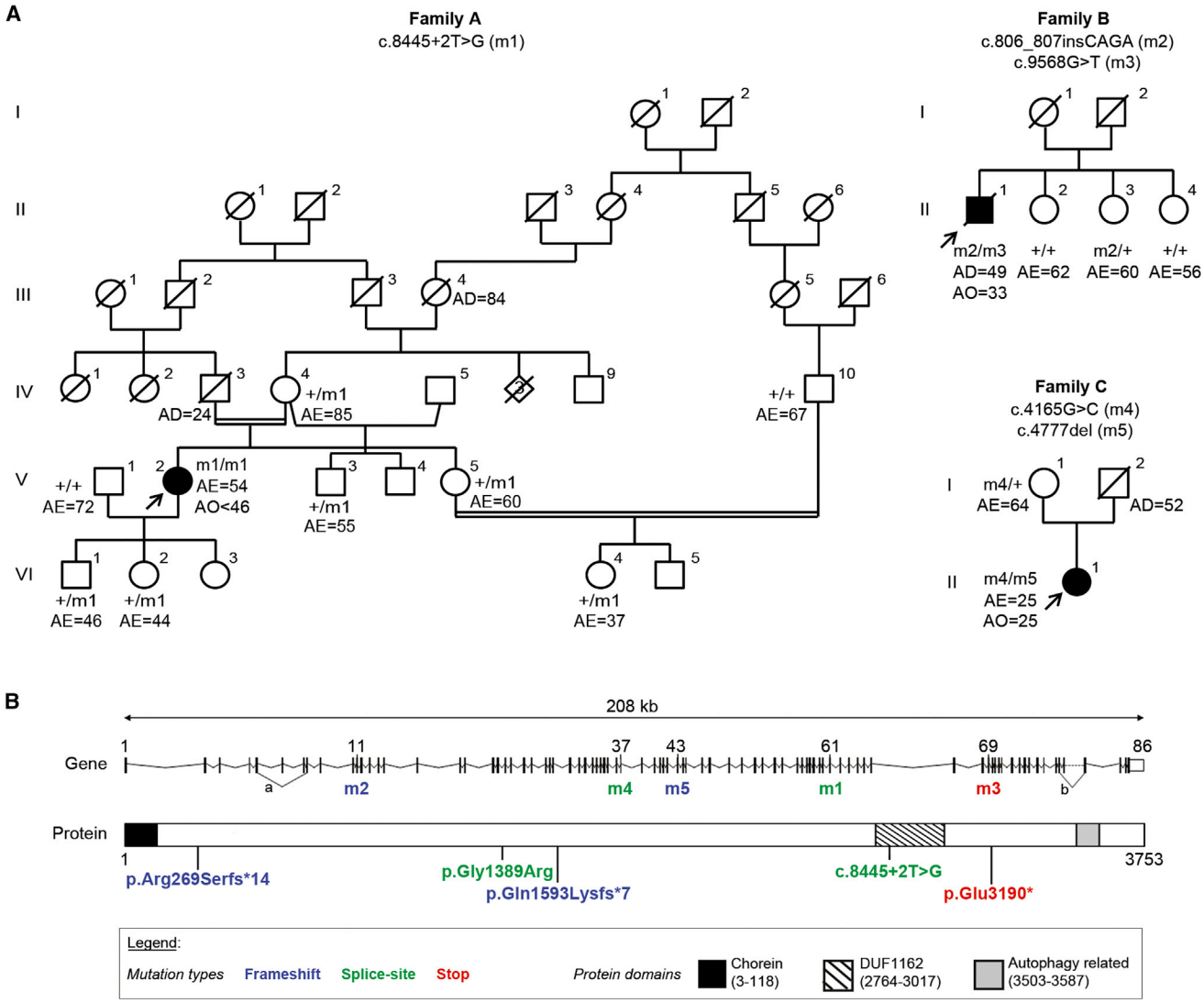

Figure 1. Identification of *VPS13C* Mutations

(A) Pedigrees of families with *VPS13C* mutations. Black symbols represent individuals with PD, open symbols, those unaffected. Arrows point to probands who underwent whole-exome sequencing. Abbreviations are as follows: AE, age at examination; AD, age at death; AO, age at onset.

(B) Schematic representation of *VPS13C* and its variations. *VPS13C* spans 208 kb and contains 86 exons encoding a 3,753-amino acid protein with a chorein domain at its N terminus, a DUF1162 domain of unknown function, and a putative autophagy-related domain. The five variations found in the three probands are indicated. Numbers above the gene identify the exons containing *VPS13C* variations. Alternative splicing a and b represent skipping of exons 6+7 and of exon 82, respectively. Transcripts 1A, GenBank: NM_017684.4: splicing a + b; 2A, GenBank: NM_020821.2: splicing b; 1B, GenBank: NM_018080.3: ends at exon 82; 2B, GenBank: NM_001018088.2: splicing a and ends at exon 82.

An in-house pipeline crossed the output data from IVA and Homozygosity Mapping to filter and identify the variants of interest (Figure S2). These variants were visualized with the Broad Institute Integrative Genomics Viewer (IGV) and verified by bidirectional Sanger sequencing using primers designed with Primer3 (Table S2) on an ABI 3730 automated sequencer (Life Technologies). Sanger sequencing confirmed the absence of mutations in origin-matched controls and determined the genetic status of unaffected relatives. Mutation nomenclature follows Human Genome Variation Society (HGVS) recommendations: the longest *VPS13C* transcript 2A cDNA nucleotides ("c.") are numbered from the adenine of the first ATG translation initiation codon as nucleotide +1 (reference sequence GenBank: NM_020821.2).

Splicing Defect Analysis by RT-PCR

Keratinocytes from affected individual V-2 in family A or peripheral blood lymphocytes from affected individual II-1 in family C (Figure 1) were used for splicing defects analyses. Hair follicles were plucked under sterile conditions and cultured in flasks coated with MG (1:10, Corning). Keratinocytes were grown on 20 mg/mL collagen IV (Sigma-Aldrich)-coated dishes containing EpiLife medium with the HKGS supplement (Life Technologies). Total RNA extraction was carried out with the RNeasy Kit (QIAGEN), according to the manufacture's manual. RNA (250 ng) was reverse transcribed into cDNA using iScript reverse transcription supermix (Bio-Rad). Primers are listed in Table S2. RT-PCR products were Sanger sequenced

directly or after sub-cloning into the pJET1.2/blunt vector (Thermo Scientific).

Studies in Mammalian Cells

Mammalian Expression Vectors, siRNAs, Cell Culture, and Transfection

COS-7 and HEK293T cells were grown in Dulbecco's Modified Eagle Medium + Glutamax (Life Technologies) supplemented with 10% goat serum (Life Technologies) and 1% penicillin-streptomycin (Life Technologies). Cells were plated, at 80% confluence, on glass coverslips (Thermo Scientific) in 24-well cell plates for immunofluorescence, 6-well plates for qPCR, 10-cm Petri dishes for subcellular fractionation by differential centrifugation and for the mitochondrion isolation kit, or 75-cm^2 flasks for continuous sucrose gradient and Percoll gradient purification. Cells were co-transfected with siRNAs (15 to 30 nM) and expression vectors using Lipofectamine 2000 (Life Technologies), in an antibiotic-free medium, according to the manufacturer's instructions. The siRNA used were: Hs_VPS13C_5 and Hs_VPS13C_6 (si*VPS13C*, QIAGEN); PINK1 stealth siRNAs (si*PINK1*, Invitrogen); and AllStars negative control siRNA (siControl, QIAGEN). Their efficacy was controlled by quantitative real-time RT-PCR (Figure 5F). The expression vectors were: pcDNA3-HA-PARK2, pcDNA3-HA-PINK1, pcDNA3-HA,[17] and pEGFP-C1 (Life Technologies). Where indicated, the cells were incubated with 10 μM CCCP (Sigma).

Subcellular Fractionation, Trypsin Digestion Assay, and Western Blot Analyses

For sucrose density gradient, confluent HEK293T cells from five 75-cm^2 flasks were harvested and disrupted with a Dounce homogenizer (80 manual strokes) in 10 mM Tris-HCl buffer (pH 7.6) containing 10% w/v sucrose, 10 mM ethylenediaminetetraacetic acid (EDTA), 0.5 mM dithiothreitol (DTT), supplemented with protease and phosphatase inhibitors (0.2 mM sodium orthovanadate, 4 mg/mL sodium fluoride, 5.4 mg/mL β-glycerophosphate, and Complete cocktail 1X – 11836145001, Roche). After three centrifugations at 600 × *g* for 5 min to remove cell debris, the cell lysate was layered on a 20%–60% linear sucrose gradient in Tris-HCl (pH 7.6) containing 10 mM EDTA, as previously described.[18] After 18 hr of centrifugation at 100,000 × *g*, successive 0.8 mL fractions were collected. Proteins were precipitated on ice with 10% trichloroacetic acid, pelleted by centrifugation at 13,000 × *g* for 45 min, and resuspended in 100 μL of loading buffer (Tris 60 mM [pH 6.8], SDS 4%, β-mercaptoethanol 5%, glycerol, and bromophenol blue).

Total protein fractions were obtained from cells lysed in 210 mM mannitol, 70 mM sucrose, 5 mM Tris (pH 7.4), 0.2 mM EGTA, 0.1 mM EDTA, 0.5 mM DTT, 0.1% BSA, and protease and phosphatase inhibitors after centrifugation at 600 × *g* for 5 min at room temperature. Mitochondrion-enriched fractions were obtained by differential centrifugation (HEK293T) or magnetic isolation (COS-7) and digested with trypsin (Sigma), as previously described.[17,19]

For isolation of pure mitochondria, cells were lysed in 250 mM mannitol, 5 mM HEPES (pH 7.4), 5 mM EGTA with protease, and phosphatase inhibitors and the crude mitochondrial fraction was layered on top of a 30% Percoll gradient, as previously described.[20] Protein concentrations were determined with Bio-Rad protein assays (Bio-Rad, 500-0006), based on the Bradford method. Samples were boiled in protein sample buffer, resolved by SDS-PAGE, transferred onto a nitrocellulose membrane (Protran, Whatman), and analyzed by Western blotting with selected primary and secondary antibodies (Table S3). Membranes were incubated with enhanced chemiluminescence substrate (Pierce); chemiluminescent and fluorescent signals were revealed on film (ECL, Amersham Hyperfilm) or captured with Odyssey Imaging (Li-COR) systems and quantified with ImageJ software (NIH). Total or cytoplasmic fractions were normalized to α-tubulin, mitochondrial fractions to PMPCB. Three to six independent fractionation experiments were quantified.

Analysis of Mitochondrial Respiration

Cellular oxygen consumption was measured via high-resolution respirometry (OROBOROS Oxygraph-2k) in a temperature-regulated chamber at 37°C. Oxygen consumption was measured in intact COS-7 cells at a density of 2.5 × 10^6 cells in 2 mL of respiration assay medium (1× DMEM, GlutaMAX, GIBCO) containing 4.5 g/L D-glucose and 4 mM L-glutamine, by sequential additions of 1 μg/mL oligomycin, 2.5 μM CCCP, and 5 μM rotenone/10 μM antimycin A. We determined the following mitochondrial parameters: basal oxygen consumption (= basal cellular respiration − non-mitochondrial respiration), proton leak (= oligomycin-inhibited respiration − non-mitochondrial respiration), maximal respiratory capacity (= maximal uncoupled respiration − non-mitochondrial respiration), reserve respiratory capacity (= maximal uncoupled respiration − basal respiration), and non-mitochondrial respiration (rotenone/antimycin A-inhibited respiration). Cells were then lysed to quantify the protein content using the Bradford reagent, which was used to normalize the oxygen consumption data. The results were expressed in pmol of O_2/s/mg of total protein.

Immunostaining, ΔΨmt, Respiration, Mitochondrial Morphology, and Parkin-Dependent Mitophagy

Immunocytochemical stainings were performed as described previously with the antibodies and dilution conditions indicated in Table S3. Changes in ΔΨmt were evaluated with the potentiometric dye tetramethylrhodamine methyl ester (TMRM) as described.[19] Mitochondrial morphology was analyzed on COS-7 cells immunostained for the Beta subunit of the mitochondrial processing peptidase (PMPCB) using an image-processing algorithm and two descriptive parameters to assess mitochondrial length and branching: aspect ratio, calculated as the ratio between major and minor axes of each mitochondrial object, representing its length; and form factor, calculated as perimeter^2/(4π × area), representing a combined evaluation of the length and degree of branching of the mitochondrial network.[21,22] For Parkin-dependent mitophagy, cells were immunostained for PMPCB or the outer mitochondrial membrane protein TOMM20 and quantified as described.[17] Images were acquired with an Olympus FV-1000 confocal microscope (×60 oil immersion objective, NA 1.35) and analyzed with ImageJ analysis software (NIH).

Quantitative Real-Time RT-PCR

To demonstrate the efficiency of the siRNA-mediated silencing of endogenous *VPS13C* in HEK293T cells, total RNA was isolated from cells transfected with control or *VPS13C* or *PINK1* siRNA using the RNeasy plus Mini Kit (QIAGEN) and QIAshredder (QIAGEN). RNA from each sample (500 ng) was reverse transcribed into cDNA using iScript reverse transcription supermix (Bio-Rad). Real-time PCR was performed with the LightCycler 480 System (Roche Applied Science) and SsoAdvanced Universal SYBR Green Supermix (Bio-Rad). Results were analyzed with LightCycler 480 sw 1.5 quantification Software (Roche Applied Science). *Beta-actin* (ACTB) was used as the reference gene for normalization. Primers are listed in Table S2.

Statistical Analysis

Statistical significance was established at $p < 0.05$ and determined with an unpaired t test in Figures 4A (Aspect Ratio) and S6A; matched t test in Figures 4C, 5B, and 5D; Mann-Whitney-Wilcoxon test in Figure 4A (Form Factor); one-way ANOVA in Figures 6 and S5; or two-way ANOVA in Figures 4B, 5E, and 5F.

Results

Truncating Mutations in *VPS13C* Cause AR Parkinsonism

Genome-wide screens in an initial series of 66 affected and 39 unaffected subjects using DNA microarrays identified a mean of 16.3 regions of homozygosity $\geq$ 2 Mb on the 22 autosomes of each consanguineous individual (gene discovery cohort). No rare deleterious large genomic rearrangements were detected. Exomes were subsequently sequenced in the 62 affected individuals with confirmed consanguinity (inbreeding coefficient $F \neq 0$) and 10 unaffected family members to identify homozygous variants which: (1) in priority, would disrupt the protein function (frameshifts, stop codons, or splicing variants); (2) were rare (minor allele frequency [MAF] < 1%) in dbSNP137, the National Heart Lung and Blood Institute (NHBLI), Exome Sequencing Project (ESP) database, and the 1000 Genomes Project; (3) were shared by affected siblings when available; (4) were heterozygous in parents and/or heterozygous or wild-type in unaffected siblings when available; (5) fell within homozygous intervals; and (6) were absent in the homozygous state from DNA of 530 controls. We identified rare or undescribed homozygous truncating variants within 32 genes, each found in a single affected individual with consanguinity that fulfilled all these prioritization criteria (Table S4). We screened these candidate genes for additional homozygous or compound heterozygous mutations in a validation cohort. *VPS13C* (also known as KIAA1421; GenBank: NM_020821.2) on chr15q22 was mutated in a consanguineous Turkish PD-affected individual (V-2 in family A) from the gene discovery cohort and in two additional French PD-affected isolated individuals (II.1 in family B and II.1 in family C) from the validation cohort (Figure 1A). In addition, we identified a total of 80 rare (MAF < 1% in public databases) single heterozygous mostly nonsynonymous variants in *VPS13C* from the validation cohort, including 14 present in at least one of the 530 European control subjects (Table S5). No additional homozygous or compound heterozygous variants were found in the 31 other candidate genes.

The affected individual V-2 in family A harbored a homozygous splice-site mutation c.8445+2T>G, intron 61 in *VPS13C* confirmed by Sanger sequencing; eight unaffected relatives, including the mother, had heterozygous c.8445+2T>G mutations or wild-type sequences (Figures 1A and S3A). Affected individuals in families B and C were compound heterozygotes (Figures 1A, S3B, and S3C): the affected individual II-1 in family B with c.[806_807insCAGA];[9568G>T], p.[Arg269Serfs*14];[Glu3190*] variants; the affected individual II-1 in family C with c.[4165G>C];[4777delC], p.[Gly1389Arg];[Gln1593Lysfs*7] variants. Direct sequencing of *VPS13C* in the three unaffected siblings (II-2, II-3, and II-4) in family B and the unaffected mother (I-1) in family C showed that they all carried heterozygous mutations or wild-type alleles (Figures 1A and S3), indicating that all variations were located on different alleles. The five *VPS13C* variants were absent from dbSNP137, 1000 Genomes Project, EVS (Table S6A), Exome Aggregation Consortium (ExAC) databases (Table S6B), and our European control exomes, except for the missense p.Gly1389Arg variant found on one control chromosome. In addition, the c.8445+2T>G mutation was absent from 200 Turkish control chromosomes. No disruptive bi-allelic variants were found in our 530 control subjects; one disruptive homozygous variant (rs199602573) was found in the EVS database and ExAC populations (1/6,246 and 2/61,547, respectively), indicating that *VPS13C* homozygous disruptive variants are extremely rare in non-PD-affected populations (Tables S6 and S7).

The c.4165G>C and c.8445+2T>G mutations were predicted in silico to modify donor splice sites, one base upstream and two bases downstream, respectively, of splice junctions (Figure S4A). Reverse-transcription PCR analysis of potential splicing defects confirmed the predictions (Figure S4B). RNA from the homozygous individual of family A showed at least three shorter transcripts, lacking up to 231 nucleotides at the end of the exon 61. In the subject with the heterozygous variant, shorter transcripts were barely visible, probably due to a high instability of these aberrant RNAs. In family C, the longer transcript was found in the subject with the heterozygous variant, containing 14 additional nucleotides from intron 37.

VPS13C contains 86 exons spanning a 208-kb genomic region and has two main transcript variants, 1A (GenBank: NM_017684.4) and 2A (GenBank: NM_020821.2) (Figure 1B). Although the transcript 1A, lacking exons 6 and 7 and encoding a 3,710-amino acid protein, is expressed in most tissues, including brain and peripheral blood cells, the longest transcript 2A encodes a brain-specific 3,753-amino acid protein.[23] Two additional isoforms with uncharacterized expression pattern are reported in Ensembl (GenBank: NM_018080.3 and NM_001018088.2) and lack the last four exons. All the isoforms contain the splice site variants found in families A and C. VPS13C contains a chorein domain at its N terminus, a DUF1162 domain of unknown function, and a putative autophagy-related domain (Figure 1B). Except for the c.8445+2T>G variant, which is located in the DUF1162 domain, none of the variants were found in the predicted domains.

Clinical and Pathological Characteristics of Affected Individuals Harboring *VPS13C* Mutations

The three affected individuals harboring *VPS13C* mutations had early disease onset (25 to <46 years) and typical parkinsonism (akineto-rigid syndrome, rest tremor, good

Table 1. Clinical Characteristics of Affected Individuals Harboring *VPS13C* Mutations

	V-2 from Family A	II-1 from Family B	II-1 from Family C
Origin	Turkish	French	French
Consanguinity	yes	no	no
Gender	female	male	female
Age at onset (years)	<46	33	25
Symptoms at onset	depression; asymetric akineto rigid syndrome; no dystonia	asymetric akineto rigid syndrome and rest tremor; limb dystonia	asymetric akineto rigid syndrome; limb dystonia
Response to levodopa	yes, partial	yes, at early stage	yes, at early stage (evaluated at 75% initially)
Complications with treatment	no motor fluctuation nor dyskinesia	fluctuation and dyskinesia, ICD, somnolence	no motor fluctuation nor dyskinesia
Evolution	severe with early cognitive decline with spatial disorientation (MMSE 21), slurred speech and hallucinations at the age of 51; axial symptoms (postural instability, FOG, and falls) and dysautonomia with urinary incontinence at the age of 54; bedridden, unable to speak, apathetic, confused, cachexic with dysphagia at the age of 58	severe with early cognitive decline (MMSE 18 at the age of 40); axial symptoms (FOG at the age of 35, falls at the age of 39); dysautonomia (at the age of 35); bedridden at the age of 43, death at the age of 49 of aspiration pneumonia	severe with early cognitive decline, slurred speech before the age of 39; severe axial symptoms at early stage; bedridden at the age of 31; gastrostomia at the age of 37. Subject's father died at 52 of a pancreatic cancer
Atypical symptoms associated	brisk tendon reflexes on the lower limbs but no pyramidal syndrome	motor neuron signs with pyramidal syndrome and limb atrophy at late stage	motor neuron signs with spastic tetraplegia
Cerebral MRI	asymmetric atrophy in frontal, parietal, and temporal areas at the expense of the left side	normal (performed at early stage)	normal (performed at early stage)

Abbreviations are as follows: ICD, impulse control disorder; MMSE, mini-mental state examination; FOG, freezing of gait.

levodopa response). Disease progression, however, was particularly severe, with early cognitive decline, loss of response to treatment, axial symptoms, and dysautonomia. Affected subjects were bedridden within 15 years of clinical onset. Pyramidal signs and motor deficits were observed in two affected individuals. Brain MRI was normal early in the disease, and then bilateral atrophy was observed in the frontal, parietal, and temporal lobes (Table 1). Post-mortem examination of the brain of the affected individual II-1 in family B, who died at age 49 of aspiration pneumonia, showed mild frontal atrophy, including the primary motor area (Figures 2A–2C). The pathology resembled diffuse Lewy body disease. Alpha-synuclein and ubiquitin positive-Lewy bodies were observed in the brainstem, limbic system, hippocampus, and all cortical associative areas, including the parieto-occipital region (Figures 2D–2F, Table S8). Tau-immunoreactive neurofibrillary tangles and neurites were seen in the brainstem, hippocampus, and primary motor cortex (Figure 2G, Table S8). There were no glial-, α-synuclein-, Aβ-, or TDP-43-immunoreactive inclusions.

Loss of *VPS13C* Function Affects Mitochondrial Morphology, Transmembrane Potential, and Respiration

To investigate the function of VPS13C, we explored its subcellular distribution in human HEK293T by sucrose gradient fractionation (Figure 3A). VPS13C was enriched in the low-density fractions 1 and 2 containing the early endosomal marker EEA1 and most of the cytosolic protein Parkin. VPS13C was also found in higher-density fractions containing membrane and soluble markers of the Golgi apparatus (GOLGA2), the ER (Calnexin, BiP), and mitochondria (TOMM70, PMPCB, PINK1). Here, it was most abundant in fractions 8–10, containing the greatest proportion of TOMM70 and PMPCB. The mitochondrial localization of VPS13C was confirmed in mitochondrion-enriched fractions and pure mitochondria from HEK293T and COS-7 cells (Figures 3B and 3C). Limited trypsin digestion of mitochondrion-enriched fractions caused concomitant loss of VPS13C and the outer mitochondrial membrane receptor TOMM70 under conditions preserving the outer mitochondrial membrane channel TOMM40 and mitochondrial matrix enzyme PMPCB, indicating that VPS13C is located on the mitochondrial surface (Figure 3C).

We then investigated the impact of loss of *VPS13C* function on mitochondrial morphology, transmembrane potential, and respiration, reported to be affected in models of *PINK1* or *PARK2* deficiency.[24,25] The siRNA-mediated silencing of *VPS13C* in COS-7 cells reduced *VPS13C* mRNA levels to no more than 25% of the control condition (Figure S6) and was associated with perinuclear redistribution of mitochondria and mitochondrial

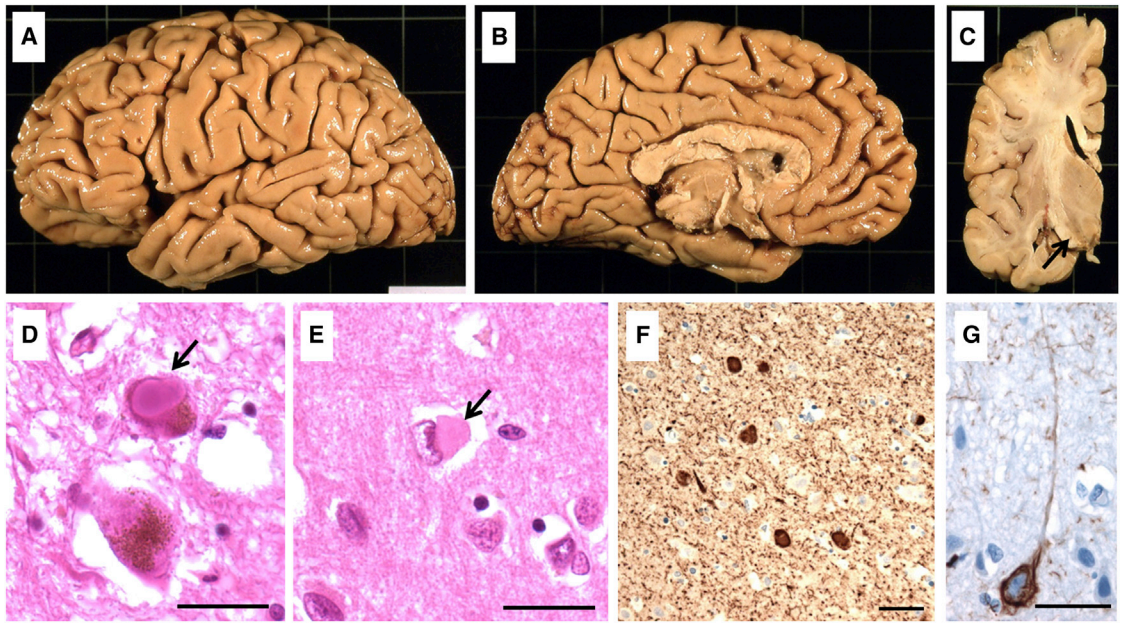

Figure 2. Neuropathology in the Proband of Family B with c.[806_807insCAGA];[9568G>T] *VPS13C* Mutations Shows Abundant α-Synucleinopathy

(A–C) Macroscopic appearance of the left hemisphere (fixed): lateral view (A); medial view (B); coronal section at the level of the cerebral peduncle (C).

(D and E) Lewy bodies in pigmented neurons in the substantia nigra (D, arrow, hematoxylin-eosin [HE] staining) and the parietal neocortex (E, arrowhead, HE staining).

(F) Representative image of α-synuclein immunoreactivity in the frontal cortex showing abundant Lewy bodies and neurites.

(G) Tau-immunoreactive neurofibrillary tangles in the primary motor cortex.

Scale bars for microscopic images represent 50 μm.

fragmentation, as confirmed by quantitative image analysis (Figure 4A). Evaluation of the mitochondrial transmembrane potential ($\Delta\Psi$mt) with the potentiometric dye tetramethylrhodamine methyl ester (TMRM) revealed a significant decrease in the mean fluorescence intensity of mitochondria in cells depleted of VPS13C (Figure 4B). The $\Delta\Psi$mt decrease was accompanied by an increase in maximal respiration rates and respiratory reserve, as assessed by high-resolution respirometry in intact cells (Figure 4C). Similar results were obtained in HEK293T cells (data not shown).

Loss of *VPS13C* Function Exacerbates PINK1/Parkin-Dependent Responses to Mitochondrial Depolarization

We further investigated the relationship between *VPS13C* and *PINK1* and *PARK2*, both at the transcript and protein levels, with respect to their well-characterized response to mitochondrial damage. PINK1 accumulates on mitochondria and recruits Parkin to initiate mitophagy in response to mitochondrial dysfunction.[4] Mitochondrial depolarization, triggered by the protonophore CCCP, partially redistributed VPS13C from mitochondria to the cytoplasm without significantly changing *VPS13C* transcript levels (Figures 5A, 5B, and 5F, left); under these conditions, PINK1 accumulated on mitochondria, as expected.[4] *VPS13C* silencing did not affect PINK1 levels under basal conditions, but it exacerbated CCCP-induced mitochondrial accumulation of PINK1 without impacting *PINK1* mRNA abundance (Figures 5C, 5D, and 5F, middle). Moreover, *VPS13C* silencing enhanced mitochondrial translocation of Parkin triggered by CCCP (Figures 5C and 5E). It also upregulated Parkin protein abundance in the cytosol without affecting *PARK2* transcript levels at 3 hr of CCCP treatment (Figures 5E and 5F, right). *PARK2* expression increases in response to mitochondrial damage caused by mitochondrial toxins, including CCCP.[26,27] Here, *PARK2* transcript levels tended to be higher at 48 hr of CCCP treatment (Figure 5F, right). This response was significantly enhanced after silencing of *VPS13C* or *PINK1*, suggesting greater mitochondrial damage. *PINK1* silencing was also associated with downregulation of *VPS13C* transcript levels under basal conditions (Figure 5F, left), an effect that was reversed by PINK1 overproduction (Figure S5), indicating the existence of multiple regulatory loops between VPS13C, PARK2, and PINK1. Consistent with the above described effects on PINK1 and Parkin, *VPS13C* silencing exacerbated PINK1/Parkin-mediated mitophagy triggered by CCCP in COS-7 cells, a model that we previously validated for the study of this process (Figures 6 and S6).[17,19]

Discussion

This study establishes *VPS13C* mutations as a monogenic cause of EO AR parkinsonism. Homozygous or compound

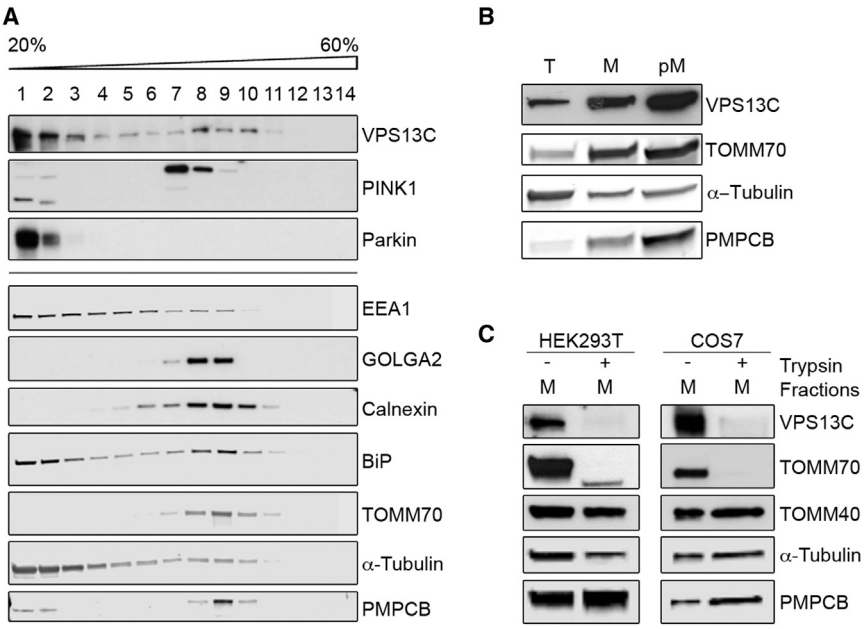

Figure 3. A Pool of VPS13C Is Located on the Outer Mitochondrial Membrane

(A) Sucrose gradient fractionation illustrating the subcellular distribution of endogenous VPS13C in HEK293T. Note the enrichment of the protein in fractions 1–3 and 8–10. Soluble endoplasmic reticulum (ER, BiP) and mitochondrial (PMPCB) markers in fractions 1 and 2 reflect organelle damage during fractionation.

(B) Western blot showing VPS13C immunoreactivity in mitochondria purified by Percoll gradient centrifugation from HEK293T cells (pM fraction). Note the enrichment in VPS13C and the mitochondrial markers TOMM70 and PMPCB in the pM fraction compared to the mitochondrion-enriched fraction (M). Abbreviation is as follows: T, total lysate.

(C) Limited trypsin treatment of mitochondrion-enriched fractions (M) from HEK293T or COS-7 cells caused loss of VPS13C and the mitochondrial surface marker TOMM70; the outer mitochondrial membrane channel TOMM40 and the matrix marker PMPCB are preserved.

heterozygous truncating mutations in three PD-affected individuals, absent from or present in the heterozygous state in available unaffected family members and in a very large number of control subjects, strongly support the pathogenicity of *VPS13C* in EO parkinsonism. We identified three affected individuals harboring *VPS13C* mutations and could not perform co-segregation analyses, due to the lack of additional affected relatives in the corresponding families. However, the affected individuals shared a specific, rare, and extremely distinctive phenotype consisting of EO parkinsonism with very rapid progression and dementia, which argues strongly for the pathogenicity of *VPS13C* mutations. The initial phenotype, EO parkinsonism and a good response to levodopa treatment, is similar to that of PD-affected individuals with *PARK2*, *PINK1*, or *DJ-1* mutations. However, the affected individuals rapidly became bedridden because of the worsening of motor dysfunction and loss of response to treatment. Dysautonomia and pyramidal signs were observed in two affected individuals, also distinguishing the phenotype from the classical, slowly progressive EO PD. The presence of numerous α-synuclein and ubiquitin-positive-Lewy bodies in the brainstem, limbic system, and many cortical areas was reminiscent of diffuse Lewy body disease, consistent with a motor phenotype associated with dementia. α-synuclein Lewy bodies are absent in most PD-affected individuals with *PARK2* mutations,[28] but were observed in the single autopsy case subject with *PINK1* mutations reported.[29] Tau-immunoreactive neurofibrillary tangles and neurites were also observed in case subjects with *PARK2* mutations.[28] These features define *VPS13C*-associated EO parkinsonism as a clinical, pathological, and genetic entity belonging to the group of synucleinopathies. In addition, our study also provides 31 potential candidate genes harboring disruptive homozygous mutations in a single PD-affected individual. However, genetic replication and functional validation are still needed to confirm their relevance to PD.

Alterations in other members of the *VPS13* family cause AR neurodegenerative disorders: *VPS13A* (MIM: 605978) (CHAC [MIM: 200150]) is mutated in chorea-acanthocytosis characterized by progressive neurodegeneration and red cell acanthocytosis,[30] and *VPS13B* (MIM: 607817) (COH1 [MIM: 216550]) is mutated in Cohen syndrome characterized by psychomotor retardation, microencephaly, and eye abnormalities.[31] *VPS13A*, *VPS13B*, and *VPS13C* are also mutated in gastric and colorectal cancers with unstable microsatellites.[32]

VPS13C belongs to a family of large VPS13 proteins (VPS13A–D) similar to yeast Vps13p.[23] Like yeast Vps, mammalian vacuolar sorting proteins are crucial for vesicular transport.[33] Initial studies linked yeast VPS13 orthologs to the delivery of proteins to the vacuole, the mammalian lysosome equivalent.[34] Mutations in *VPS35*, encoding a core component of the retromer complex regulating endosomal protein sorting, are implicated in AD late-onset PD.[35,36] VPS35 is also involved in protein trafficking from mitochondria to peroxisomes through mitochondria-derived vesicles.[37] PINK1 and Parkin play a role in this transport route, which delivers damaged mitochondrial cargo directly to lysosomes in response to mitochondrial stress.[6] However, the machinery regulating cargo selection and sorting into vesicles remains to be identified. VPS13C might be involved in this process. Such a mechanism would be consistent with its mitochondrial localization and the observed relocation to the cytosol in response to mitochondrial damage.

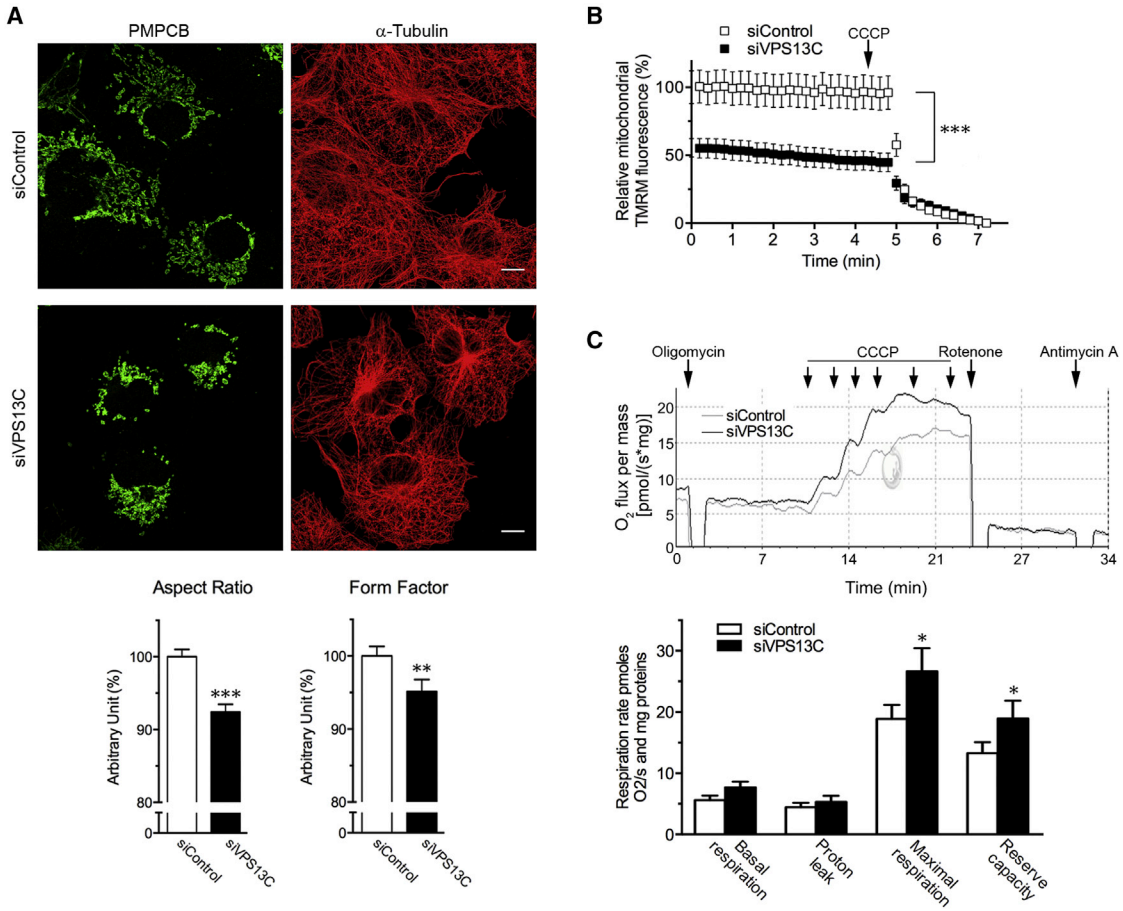

Figure 4. *VPS13C* Silencing Impacts Mitochondrial Morphology, Transmembrane Potential, and Respiration

(A) Representative immunofluorescence staining illustrating mitochondrial perinuclear redistribution and fragmentation in COS-7 cells silenced for *VPS13C* (si*VPS13C*, 30 nM) compared to cells treated with control siRNA (siControl, 30 nM): green, mitochondrial matrix marker PMPCB; red, α-Tubulin. *VPS13C* silencing reduced *VPS13C* mRNA levels to no more than 25% of the control condition (see Figure S6). Scale bars represent 10 μm. Quantification of aspect ratio and form factor (see Subjects and Methods, Koopman et al.[21], and Buhlman et al.[22]) shows reduced mitochondrial network complexity in si*VPS13C*-treated cells (means ± SEM; **$p < 0.01$; ***$p < 0.001$, of $n = 88$ or 86 cells scored per condition).

(B) Analysis of the relative TMRM fluorescence of mitochondria in COS-7 cells transfected as in (A), illustrating the decrease in ΔΨmt in cells depleted for VPS13C. $n = 40$ cells per condition from one experiment representative of three carried out. ***$p < 0.001$.

(C) Oxygen consumption rates in intact COS-7 cells transfected with siControl or si*VPS13C*. The top panel shows the oxygen flux corrected for instrumental background from one representative experiment. The graph in the bottom panel displays the respiration rates. Absence of *VPS13C* is associated with increased maximal respiration (= maximal uncoupled respiration under CCCP − non-mitochondrial respiration in the presence of the mitochondrial complex I and III inhibitors, rotenone, and antimycin A) and reserve capacity (= maximal uncoupled respiration − basal respiration before the addition of the complex V inhibitor oligomycin). Means ± SEM; *$p < 0.05$, of six independent experiments.

Several other observations in mammalian cells suggest that, like PINK1 and Parkin, VPS13C plays a role in mitochondrial maintenance. VPS13C depletion led to reduction of ΔΨmt and mitochondrial fragmentation in cell lines. Moreover, it enhanced maximal respiration rates, suggesting compensatory adaptation aimed at preserving ΔΨmt levels. In neuronal cells, which produce ATP mainly through mitochondrial oxidative phosphorylation and are unable to switch to glycolysis under acute mitochondrial stress, such changes might in the long term exacerbate generation of reactive oxygen species and trigger irreversible mitochondrial damage.[38,39] VPS13C depletion also upregulated PINK1/Parkin-dependent mitophagy, and, similarly to PINK1 depletion, it enhanced the previously reported transcriptional upregulation of Parkin in response to toxin-induced mitochondrial dysfunction. Overall, these data suggest that loss of *VPS13C* function increases mitochondrial vulnerability to stress and thereby activates PINK1/Parkin-dependent mitochondrial quality control pathways. Based on the inverse relationship between VPS13C and PINK1 protein levels on the mitochondrial surface, we cannot exclude that VPS13C also acts as a negative regulator of PINK1.

Mitochondrial function is ensured by a series of interconnected finely orchestrated pathways, activated in response to different degrees of mitochondrial dysfunction.[40] Excessive mitophagy has been associated with α-synuclein-dependent neurodegeneration.[41] Further work is required

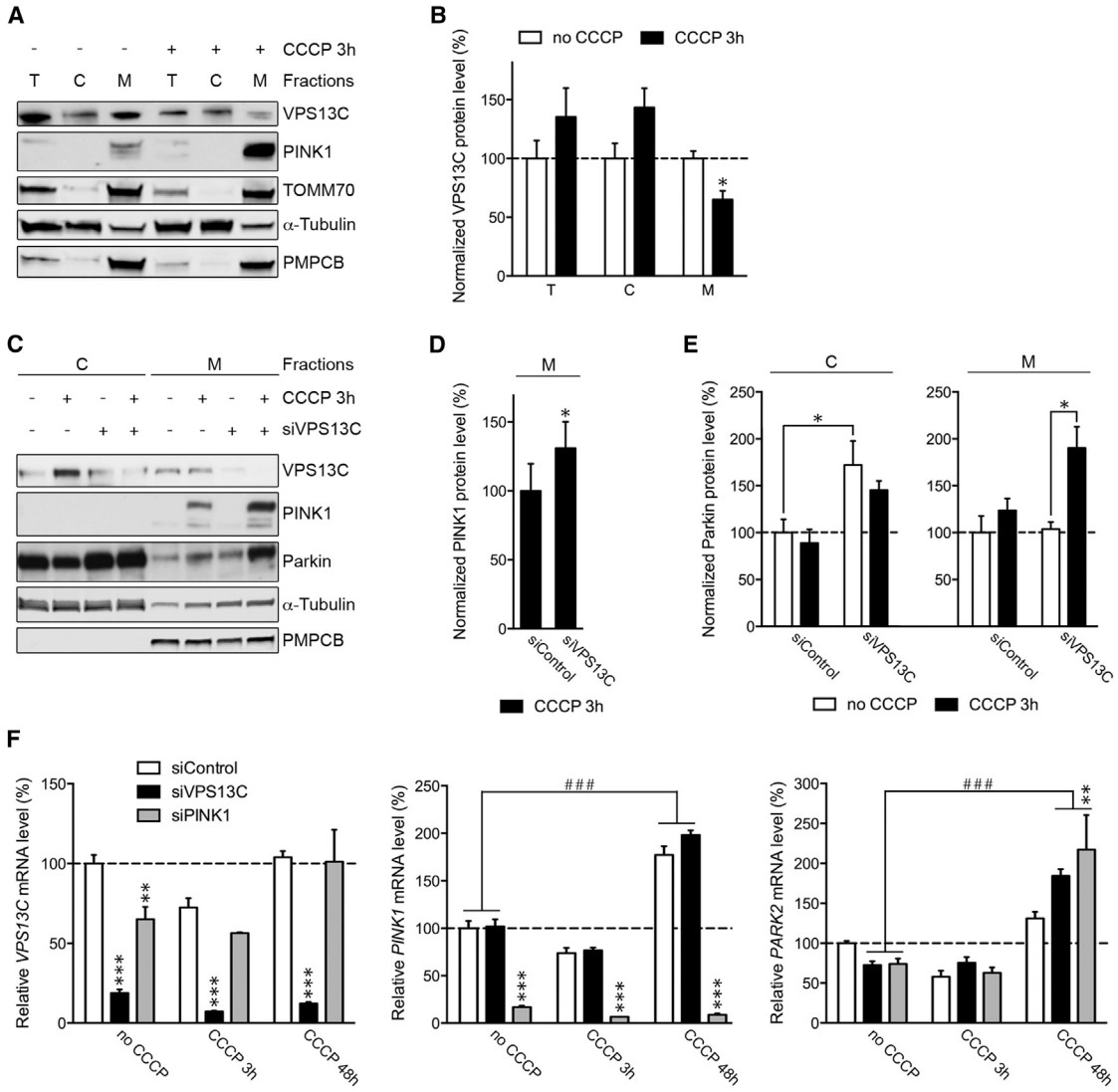

Figure 5. Loss of VPS13C Function Enhances Mitochondrial Accumulation of PINK1, Recruitment of Parkin, and *PARK2* Upregulation in Response to CCCP

(A and B) Western blot (A) and corresponding VPS13C protein levels (B) (normalized to α-Tubulin or PMPCB) in cytosolic (C), mitochondrion-enriched (M), and total (T) cell fractions from HEK293T cells treated or not with CCCP (10 μM, 3 hr). VPS13C levels decreased significantly in mitochondria after CCCP treatment, but tended to increase in cytosol (means ± SEM; *$p < 0.05$, of six independent fractionation experiments).

(C–E) Western blot (C) and corresponding normalized protein levels (D, E) in cytosolic and mitochondrion-enriched fractions from HEK293T transfected with 30 nM of control siRNA (siControl) or siRNA targeting *VPS13C* (si*VPS13C*).

(D) CCCP treatment resulted in accumulation of PINK1 (endogenous) in mitochondrion-enriched fractions (M) after treatment with siControl (–) and, more significantly, with si*VPS13C* (+).

(E) Accumulation of Parkin (endogenous) on depolarized mitochondria was also strongly enhanced in cells treated with si*VPS13C*. In addition, Parkin levels were upregulated in the cytosolic (C) fractions, particularly in untreated cells (means ± SEM; *$p < 0.05$ of four independent fractionation experiments).

(F) Quantitative real-time RT-PCR showing relative mRNA levels, normalized to α-actin (*ACTB*), in HEK293T cells treated with control siRNA (siControl), or siRNA targeting *VPS13C* (si*VPS13C*) or *PINK1* (si*PINK1*), under basal conditions or after CCCP treatment. Note the more than 30% decrease in *VPS13C* mRNA levels after *PINK1* silencing under basal conditions, but not after CCCP treatment (left). Note also that *VPS13C* and *PINK1* silencing enhance the upregulation of *PARK2* mRNA at 48 hr of CCCP treatment (right); means ± SEM of three to nine replicates per condition from two independent experiments (**$p < 0.01$; ***$p < 0.001$ compared to siControl within each condition of CCCP treatment; ###$p < 0.001$ between the indicated conditions of CCCP treatments).

to clarify the role of VPS13C in mitochondrial maintenance and dissect its possible relation to PINK1/Parkin-dependent pathways.

Enrichment of VPS13C in cell fractions containing the early endosomal marker EEA1 suggests broader roles for VPS13C in vesicular trafficking. A more general involvement in endosomal-lysosomal trafficking, possibly counteracting α-synuclein pathology as recently reported for VPS35,[42] might explain the diffuse α-synuclein pathology and rapid progression to dementia in individuals with *VPS13C*

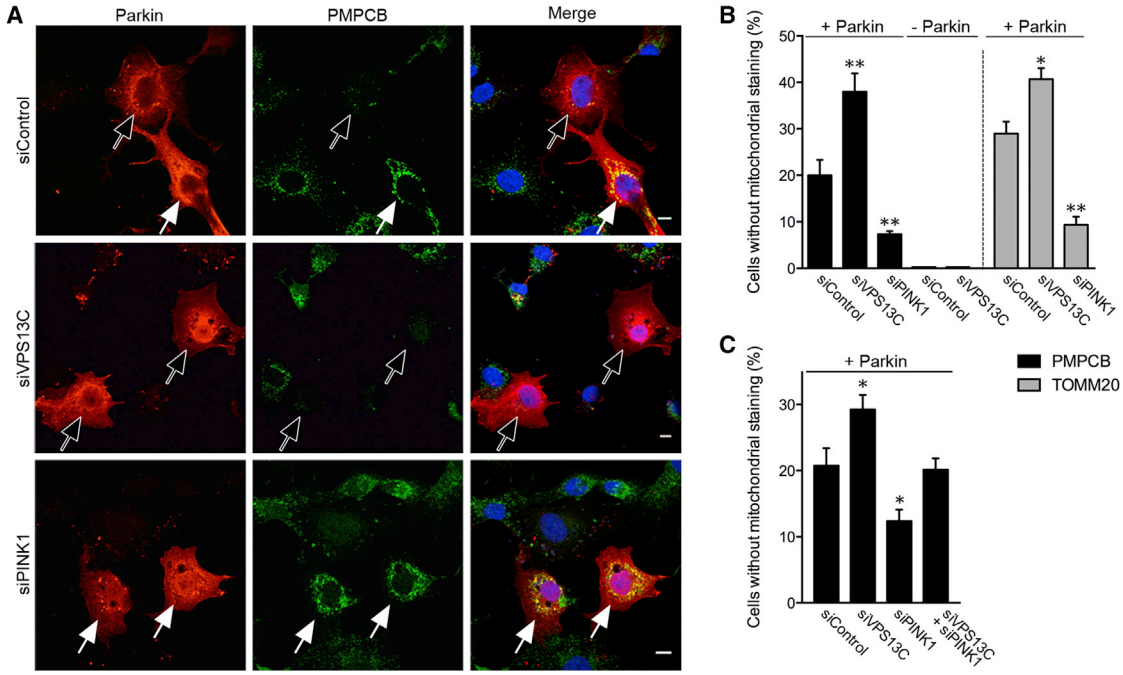

Figure 6. Loss of *VPS13C* Function Exacerbates PINK1/Parkin-Dependent Mitophagy

(A) Immunofluorescence staining of a representative experiment illustrating PINK1/Parkin-dependent mitophagy in COS-7 cells overproducing Parkin and silenced for *VPS13C* or *PINK1* (20 nM siRNA) after CCCP treatment (10 μM for 48 hr): red, Parkin; green, mitochondrial matrix marker PMPCB. Open arrows indicate loss of mitochondrial networks; white arrows show preserved networks. Scale bars represent 10 μm.

(B) Quantification of mitophagy in the conditions described in (A), expressed as the proportion of COS-7 cells without PMPCB (black bars) or TOMM20 (gray bars) staining; the si*VPS13C* treatment increased and si*PINK1* decreased the proportion. In the absence of exogenous Parkin (−Parkin; cells overproducing the control protein EGFP) or CCCP (not shown), all the cells harbored normal mitochondrial PMPCB staining, whether or not *VPS13C* was silenced (means ± SEM; *$p < 0.05$, **$p < 0.01$ of 3 independent experiments; 100 cells scored per condition).

(C) Proportion of COS-7 cells without PMPCB staining after transfection with half-doses (10 nM) of each siRNA and 48 hr of CCCP treatment. The mitophagy-promoting effect of *VPS13C* depletion was abolished by concomitant silencing of *PINK1* (means ± SEM; *$p < 0.05$ of 3 independent experiments; 100 cells scored per condition).

mutations. Such a mechanism would potentially represent a unifying link with cellular pathways involved in AD PD.

In summary, we describe truncating mutations in *VPS13C* associated with EO parkinsonism with rapid progression and widely distributed Lewy bodies. A meta-analysis of PD genome-wide association studies recently identified a susceptibility allele ~250 kb from *VPS13C* but not associated with either CpG methylation or mRNA expression,[43] suggesting that *VPS13C* can either cause a monogenic form of EO parkinsonism or confer genetic susceptibility to PD. Although we are confident that our work strongly implicates *VPS13C* mutations in PD, further genetic studies in other populations are needed to confirm their pathogenicity. The development of animal models in which *VPS13C* is stably inactivated will help dissect the mechanisms by which loss of *VPS13C* function affects the survival of dopaminergic neurons.

Accession Numbers

The accession numbers for the variations in *VPS13C* reported in this paper are ClinVar: SCV000262816, SCV000262817, SCV000262818, SCV000262819, and SCV000262820.

Supplemental Data

Supplemental Data include six figures and eight tables and can be found with this article online at http://dx.doi.org/10.1016/j.ajhg.2016.01.014.

Consortia

Members of The French Parkinson's Disease Genetics Study (PDG) are Suzanne Lesage, François Tison, Marie Vidailhet, Jean-Christophe Corvol, Yves Agid, Mathieu Anheim, Anne-Marie Bonnet, Michel Borg, Emmanuel Broussolle, Philippe Damier, Alain Destée, Alexandra Dürr, Franck Durif, Paul Krack, Stephan Klebe, Ebba Lohmann, Maria Martinez, Pierre Pollak, Olivier Rascol, Christine Tranchant, Marc Vérin, François Viallet, and Alexis Brice.

Members of The International Parkinson Disease Genomics Consortium (IPDGC) are Suzanne Lesage, Elisa Majounie, François Tison, Marie Vidailhet, Jean Christophe Corvol, Michael A. Nalls, Dena G. Hernandez, J. Raphael Gibbs, Alexandra Dürr, Sampath Arepalli, Roger A. Barker, Yoav Ben-Shlomo, Daniela Berg, Francesco Bettella, Kailash Bhatia, Rob M.A. de Bie, Alessandro Biffi, Bastiaan R. Bloem, Zoltan Bochdanovits, Michael Bonin, Jose M. Bras, Kathrin Brockmann, Janet Brooks, David J. Burn, Gavin Charlesworth, Honglei Chen, Patrick F. Chinnery, Sean Chong, Carl E. Clarke, Mark R. Cookson, Carl Counsell, Philippe Damier,

Jean-François Dartigues, Panos Deloukas, Günther Deuschl, David T. Dexter, Karin D. van Dijk, Allissa Dillman, Jing Dong, Frank Durif, Sarah Edkins, Valentina Escott-Price, Jonathan R. Evans, Thomas Foltynie, Jianjun Gao, Michelle Gardner, Alison Goate, Emma Gray, Rita Guerreiro, Clare Harris, Jacobus J. van Hilten, Albert Hofman, Albert Hollenbeck, Peter Holmans, Janice Holton, Michèle Hu, Xuemei Huang, Heiko Huber, Gavin Hudson, Sarah E. Hunt, Johanna Huttenlocher, Thomas Illig, Pálmi V. Jónsson, Laura L. Kilarski, Iris E. Jansen, Jean-Charles Lambert, Cordelia Langford, Andrew Lees, Peter Lichtner, Patricia Limousin, Grisel Lopez, Delia Lorenz, Steven Lubbe, Codrin Lungu, María Martinez, Walter Mätzler, Alisdair McNeill, Catriona Moorby, Matthew Moore, Karen E. Morrison, Ese Mudanohwo, Sean S. O'Sullivan, Michael J. Owen, Justin Pearson, Joel S. Perlmutter, Hjörvar Pétursson, Vincent Plagnol, Pierre Pollak, Bart Post, Simon Potter, Bernard Ravina, Tamas Revesz, Olaf Riess, Fernando Rivadeneira, Patrizia Rizzu, Mina Ryten, Mohamad Saad, Javier Simón-Sánchez, Stephen Sawcer, Anthony Schapira, Hans Scheffer, Claudia Schulte, Manu Sharma, Karen Shaw, Una-Marie Sheerin, Ira Shoulson, Joshua Shulman, Ellen Sidransky, Chris C.A. Spencer, Hreinn Stefánsson, Kári Stefánsson, Joanna D. Stockton, Amy Strange, Kevin Talbot, Carlie M. Tanner, Avazeh Tashakkori-Ghanbaria, Daniah Trabzuni, Bryan J. Traynor, André G. Uitterlinden, Daan Velseboer, Robert Walker, Bart van de Warrenburg, Mirdhu Wickremaratchi, Caroline H. Williams-Gray, Sophie Winder-Rhodes, Isabel Wurster, Nigel Williams, Huw R. Morris, Peter Heutink, John Hardy, Nicholas W. Wood, Thomas Gasser, Andrew B. Singleton, and Alexis Brice.

Acknowledgments

The authors are grateful to the families for their participation in this study. We thank Merle Ruberg for critical reading of the manuscript, the DNA and Cell Bank of ICM, the Plate-Forme d'Imagerie Cellulaire de la Pitié-Salpêtrière (PICPS), and Ebru Özer and Meltem Pak for sample preparation. We are grateful to the Lille brain bank for the gift of a brain ("Lille Neurobank," BB-0033-00030). This study was supported by the National Research Funding Agency (ANR-08-NEUR-004-01) in association with ERA-NET NEURON, the France-Parkinson Association, the Roger de Spoelberch Foundation (R12123DD), the French Academy of Sciences, the French program "Investissements d'avenir" (ANR-10-IAIHU-06), and the European Joint Programme - Neurodegenerative Disease Research (JPND-COURAGE-PD) project. This study was also supported by the Intramural Research Program of the National Institute on Aging and the National Institutes of Neurological Disorders and Stroke, NIH, Department of Health and Human Services (project Z01 AG000958 and by MRC Grant G1100643/1), by the European Social Fund, and by the Ministry of Science, Research, and the Arts, Baden-Württemberg. This work was also supported by the Department of Defense, including grant 10064005/11348001, the French Health Ministry (PHRC), France Parkinson Association, Lille University Hospital (A. Destée), the Atip/Avenir from the National Institute of Health and Medical Research (INSERM), the ANR in association with the ERA-NET E-rare program, the France Alzheimer Association, and a Career Integration Grant from Marie Curie Actions (E.K.). C.P. received a postdoctoral fellowship from the Cognacq-Jay Foundation. S.C. received postdoctoral fellowships from EMBO and AFM-Telethon.

Received: November 16, 2015
Accepted: January 20, 2016
Published: February 25, 2016

Web Resources

The URLs for data presented herein are as follows:

1000 Genomes, http://browser.1000genomes.org
ANNOVAR, http://annovar.openbioinformatics.org/en/latest/
Burrows-Wheeler Aligner, http://bio-bwa.sourceforge.net/
ClinVar, https://www.ncbi.nlm.nih.gov/clinvar/
dbSNP, http://www.ncbi.nlm.nih.gov/projects/SNP/
Ensembl Genome Browser, http://www.ensembl.org/index.html
ExAC Browser, http://exac.broadinstitute.org/
IGV, http://www.broadinstitute.org/igv/
OMIM, http://www.omim.org/
GATK, https://www.broadinstitute.org/gatk/
Human Splicing Finder, http://www.umd.be/HSF3/HSF.html
Ingenuity Variant Analysis, http://www.ingenuity.com/products/variant-analysis
MUSCLE, http://www.ebi.ac.uk/Tools/msa/muscle/
NCBI Gene, http://www.ncbi.nlm.nih.gov/gene
NHLBI Exome Sequencing Project (ESP) Exome Variant Server, http://evs.gs.washington.edu/EVS/
Picard, http://picard.sourceforge.net/
RefSeq, http://www.ncbi.nlm.nih.gov/RefSeq
Primer3, http://www.bioinformatics.nl/cgi-bin/primer3plus/primer3plus.cgi
SnpEff, http://snpeff.sourceforge.net/
SnpSift, http://snpeff.sourceforge.net/SnpSift.html
UCSC Genome Browser, http://genome.ucsc.edu

References

1. Bonifati, V. (2014). Genetics of Parkinson's disease–state of the art, 2013. Parkinsonism Relat. Disord. *20* (*Suppl 1*), S23–S28.
2. Lücking, C.B., Dürr, A., Bonifati, V., Vaughan, J., De Michele, G., Gasser, T., Harhangi, B.S., Meco, G., Denèfle, P., Wood, N.W., et al.; French Parkinson's Disease Genetics Study Group; European Consortium on Genetic Susceptibility in Parkinson's Disease (2000). Association between early-onset Parkinson's disease and mutations in the parkin gene. N. Engl. J. Med. *342*, 1560–1567.
3. Ibáñez, P., Lesage, S., Lohmann, E., Thobois, S., De Michele, G., Borg, M., Agid, Y., Dürr, A., and Brice, A.; French Parkinson's Disease Genetics Study Group (2006). Mutational analysis of the PINK1 gene in early-onset parkinsonism in Europe and North Africa. Brain *129*, 686–694.
4. Pickrell, A.M., and Youle, R.J. (2015). The roles of PINK1, parkin, and mitochondrial fidelity in Parkinson's disease. Neuron *85*, 257–273.
5. Burchell, V.S., Nelson, D.E., Sanchez-Martinez, A., Delgado-Camprubi, M., Ivatt, R.M., Pogson, J.H., Randle, S.J., Wray, S., Lewis, P.A., Houlden, H., et al. (2013). The Parkinson's disease-linked proteins Fbxo7 and Parkin interact to mediate mitophagy. Nat. Neurosci. *16*, 1257–1265.
6. McLelland, G.-L., Soubannier, V., Chen, C.X., McBride, H.M., and Fon, E.A. (2014). Parkin and PINK1 function in a vesicular trafficking pathway regulating mitochondrial quality control. EMBO J. *33*, 282–295.
7. Hughes, A.J., Daniel, S.E., Kilford, L., and Lees, A.J. (1992). Accuracy of clinical diagnosis of idiopathic Parkinson's disease: a clinico-pathological study of 100 cases. J. Neurol. Neurosurg. Psychiatry *55*, 181–184.
8. Leutenegger, A.-L., Prum, B., Génin, E., Verny, C., Lemainque, A., Clerget-Darpoux, F., and Thompson, E.A. (2003).

Estimation of the inbreeding coefficient through use of genomic data. Am. J. Hum. Genet. *73*, 516–523.
9. Buée-Scherrer, V., Condamines, O., Mourton-Gilles, C., Jakes, R., Goedert, M., Pau, B., and Delacourte, A. (1996). AD2, a phosphorylation-dependent monoclonal antibody directed against tau proteins found in Alzheimer's disease. Brain Res. Mol. Brain Res. *39*, 79–88.
10. Deramecourt, V., Lebert, F., Maurage, C.-A., Fernandez-Gomez, F.-J., Dujardin, S., Colin, M., Sergeant, N., Buée-Scherrer, V., Clot, F., Ber, I.L., et al. (2012). Clinical, neuropathological, and biochemical characterization of the novel tau mutation P332S. J. Alzheimers Dis. *31*, 741–749.
11. Li, H., and Durbin, R. (2010). Fast and accurate long-read alignment with Burrows-Wheeler transform. Bioinformatics *26*, 589–595.
12. McKenna, A., Hanna, M., Banks, E., Sivachenko, A., Cibulskis, K., Kernytsky, A., Garimella, K., Altshuler, D., Gabriel, S., Daly, M., and DePristo, M.A. (2010). The Genome Analysis Toolkit: a MapReduce framework for analyzing next-generation DNA sequencing data. Genome Res. *20*, 1297–1303.
13. Wang, K., Li, M., and Hakonarson, H. (2010). ANNOVAR: functional annotation of genetic variants from high-throughput sequencing data. Nucleic Acids Res. *38*, e164.
14. Crooks, G.E., Hon, G., Chandonia, J.-M., and Brenner, S.E. (2004). WebLogo: a sequence logo generator. Genome Res. *14*, 1188–1190.
15. Desmet, F.-O., Hamroun, D., Lalande, M., Collod-Béroud, G., Claustres, M., and Béroud, C. (2009). Human Splicing Finder: an online bioinformatics tool to predict splicing signals. Nucleic Acids Res. *37*, e67.
16. Schneider, T.D., and Stephens, R.M. (1990). Sequence logos: a new way to display consensus sequences. Nucleic Acids Res. *18*, 6097–6100.
17. Bertolin, G., Ferrando-Miguel, R., Jacoupy, M., Traver, S., Grenier, K., Greene, A.W., Dauphin, A., Waharte, F., Bayot, A., Salamero, J., et al. (2013). The TOMM machinery is a molecular switch in PINK1 and PARK2/PARKIN-dependent mitochondrial clearance. Autophagy *9*, 1801–1817.
18. Erpapazoglou, Z., Froissard, M., Nondier, I., Lesuisse, E., Haguenauer-Tsapis, R., and Belgareh-Touzé, N. (2008). Substrate- and ubiquitin-dependent trafficking of the yeast siderophore transporter Sit1. Traffic *9*, 1372–1391.
19. Bertolin, G., Jacoupy, M., Traver, S., Ferrando-Miguel, R., Saint Georges, T., Grenier, K., Ardila-Osorio, H., Muriel, M.-P., Takahashi, H., Lees, A.J., et al. (2015). Parkin maintains mitochondrial levels of the protective Parkinson's disease-related enzyme 17-β hydroxysteroid dehydrogenase type 10. Cell Death Differ. *22*, 1563–1576.
20. Wieckowski, M.R., Giorgi, C., Lebiedzinska, M., Duszynski, J., and Pinton, P. (2009). Isolation of mitochondria-associated membranes and mitochondria from animal tissues and cells. Nat. Protoc. *4*, 1582–1590.
21. Koopman, W.J.H., Verkaart, S., Visch, H.-J., van der Westhuizen, F.H., Murphy, M.P., van den Heuvel, L.W.P.J., Smeitink, J.A.M., and Willems, P.H.G.M. (2005). Inhibition of complex I of the electron transport chain causes O2-. -mediated mitochondrial outgrowth. Am. J. Physiol. Cell Physiol. *288*, C1440–C1450.
22. Buhlman, L., Damiano, M., Bertolin, G., Ferrando-Miguel, R., Lombès, A., Brice, A., and Corti, O. (2014). Functional interplay between Parkin and Drp1 in mitochondrial fission and clearance. Biochim. Biophys. Acta *1843*, 2012–2026.
23. Velayos-Baeza, A., Vettori, A., Copley, R.R., Dobson-Stone, C., and Monaco, A.P. (2004). Analysis of the human VPS13 gene family. Genomics *84*, 536–549.
24. Exner, N., Treske, B., Paquet, D., Holmström, K., Schiesling, C., Gispert, S., Carballo-Carbajal, I., Berg, D., Hoepken, H.-H., Gasser, T., et al. (2007). Loss-of-function of human PINK1 results in mitochondrial pathology and can be rescued by parkin. J. Neurosci. *27*, 12413–12418.
25. Mortiboys, H., Thomas, K.J., Koopman, W.J.H., Klaffke, S., Abou-Sleiman, P., Olpin, S., Wood, N.W., Willems, P.H.G.M., Smeitink, J.A.M., Cookson, M.R., and Bandmann, O. (2008). Mitochondrial function and morphology are impaired in parkin-mutant fibroblasts. Ann. Neurol. *64*, 555–565.
26. Henn, I.H., Bouman, L., Schlehe, J.S., Schlierf, A., Schramm, J.E., Wegener, E., Nakaso, K., Culmsee, C., Berninger, B., Krappmann, D., et al. (2007). Parkin mediates neuroprotection through activation of IkappaB kinase/nuclear factor-kappaB signaling. J. Neurosci. *27*, 1868–1878.
27. Bouman, L., Schlierf, A., Lutz, A.K., Shan, J., Deinlein, A., Kast, J., Galehdar, Z., Palmisano, V., Patenge, N., Berg, D., et al. (2011). Parkin is transcriptionally regulated by ATF4: evidence for an interconnection between mitochondrial stress and ER stress. Cell Death Differ. *18*, 769–782.
28. Doherty, K.M., Silveira-Moriyama, L., Parkkinen, L., Healy, D.G., Farrell, M., Mencacci, N.E., Ahmed, Z., Brett, F.M., Hardy, J., Quinn, N., et al. (2013). Parkin disease: a clinicopathologic entity? JAMA Neurol. *70*, 571–579.
29. Samaranch, L., Lorenzo-Betancor, O., Arbelo, J.M., Ferrer, I., Lorenzo, E., Irigoyen, J., Pastor, M.A., Marrero, C., Isla, C., Herrera-Henriquez, J., and Pastor, P. (2010). PINK1-linked parkinsonism is associated with Lewy body pathology. Brain *133*, 1128–1142.
30. Rampoldi, L., Dobson-Stone, C., Rubio, J.P., Danek, A., Chalmers, R.M., Wood, N.W., Verellen, C., Ferrer, X., Malandrini, A., Fabrizi, G.M., et al. (2001). A conserved sorting-associated protein is mutant in chorea-acanthocytosis. Nat. Genet. *28*, 119–120.
31. Kolehmainen, J., Black, G.C.M., Saarinen, A., Chandler, K., Clayton-Smith, J., Träskelin, A.-L., Perveen, R., Kivitie-Kallio, S., Norio, R., Warburg, M., et al. (2003). Cohen syndrome is caused by mutations in a novel gene, COH1, encoding a transmembrane protein with a presumed role in vesicle-mediated sorting and intracellular protein transport. Am. J. Hum. Genet. *72*, 1359–1369.
32. An, C.H., Kim, Y.R., Kim, H.S., Kim, S.S., Yoo, N.J., and Lee, S.H. (2012). Frameshift mutations of vacuolar protein sorting genes in gastric and colorectal cancers with microsatellite instability. Hum. Pathol. *43*, 40–47.
33. Richardson, S.C.W., Winistorfer, S.C., Poupon, V., Luzio, J.P., and Piper, R.C. (2004). Mammalian late vacuole protein sorting orthologues participate in early endosomal fusion and interact with the cytoskeleton. Mol. Biol. Cell *15*, 1197–1210.
34. Bankaitis, V.A., Johnson, L.M., and Emr, S.D. (1986). Isolation of yeast mutants defective in protein targeting to the vacuole. Proc. Natl. Acad. Sci. USA *83*, 9075–9079.
35. Vilariño-Güell, C., Wider, C., Ross, O.A., Dachsel, J.C., Kachergus, J.M., Lincoln, S.J., Soto-Ortolaza, A.I., Cobb, S.A., Wilhoite, G.J., Bacon, J.A., et al. (2011). VPS35 mutations in Parkinson disease. Am. J. Hum. Genet. *89*, 162–167.
36. Zimprich, A., Benet-Pagès, A., Struhal, W., Graf, E., Eck, S.H., Offman, M.N., Haubenberger, D., Spielberger, S., Schulte, E.C., Lichtner, P., et al. (2011). A mutation in VPS35, encoding

a subunit of the retromer complex, causes late-onset Parkinson disease. Am. J. Hum. Genet. *89*, 168–175.

37. Braschi, E., Goyon, V., Zunino, R., Mohanty, A., Xu, L., and McBride, H.M. (2010). Vps35 mediates vesicle transport between the mitochondria and peroxisomes. Curr. Biol. *20*, 1310–1315.
38. Almeida, A., Almeida, J., Bolaños, J.P., and Moncada, S. (2001). Different responses of astrocytes and neurons to nitric oxide: the role of glycolytically generated ATP in astrocyte protection. Proc. Natl. Acad. Sci. USA *98*, 15294–15299.
39. Almeida, A., Moncada, S., and Bolaños, J.P. (2004). Nitric oxide switches on glycolysis through the AMP protein kinase and 6-phosphofructo-2-kinase pathway. Nat. Cell Biol. *6*, 45–51.
40. Rugarli, E.I., and Langer, T. (2012). Mitochondrial quality control: a matter of life and death for neurons. EMBO J. *31*, 1336–1349.
41. Choubey, V., Safiulina, D., Vaarmann, A., Cagalinec, M., Wareski, P., Kuum, M., Zharkovsky, A., and Kaasik, A. (2011). Mutant A53T alpha-synuclein induces neuronal death by increasing mitochondrial autophagy. J. Biol. Chem. *286*, 10814–10824.
42. Dhungel, N., Eleuteri, S., Li, L.-B., Kramer, N.J., Chartron, J.W., Spencer, B., Kosberg, K., Fields, J.A., Stafa, K., Adame, A., et al. (2015). Parkinson's disease genes VPS35 and EIF4G1 interact genetically and converge on α-synuclein. Neuron *85*, 76–87.
43. Nalls, M.A., Pankratz, N., Lill, C.M., Do, C.B., Hernandez, D.G., Saad, M., DeStefano, A.L., Kara, E., Bras, J., Sharma, M., et al.; International Parkinson's Disease Genomics Consortium (IPDGC); Parkinson's Study Group (PSG) Parkinson's Research: The Organized GENetics Initiative (PROGENI); 23andMe; GenePD; NeuroGenetics Research Consortium (NGRC); Hussman Institute of Human Genomics (HIHG); Ashkenazi Jewish Dataset Investigator; Cohorts for Health and Aging Research in Genetic Epidemiology (CHARGE); North American Brain Expression Consortium (NABEC); United Kingdom Brain Expression Consortium (UKBEC); Greek Parkinson's Disease Consortium; Alzheimer Genetic Analysis Group (2014). Large-scale meta-analysis of genome-wide association data identifies six new risk loci for Parkinson's disease. Nat. Genet. *46*, 989–993.